J. Fluid Mech. (1981), *vol.* 103, *pp.* 53–63
Printed in Great Britain

Large-eddy simulation of the shear-free turbulent boundary layer

By S. BIRINGEN†
Boğaziçi University, P.K. 2 Bebek, Istanbul, Turkey

AND W. C. REYNOLDS
Stanford University, Stanford, California 94305

(Received 6 December 1978 and in revised form 20 February 1980)

The shear-free turbulent boundary layer is calculated by the large-eddy simulation technique. The filtered Navier–Stokes equations are used; the method of integration employs Fourier expansions in the homogeneous directions and finite differences in the cross-stream direction. Results indicate that the simulation is capable of predicting the primary Reynolds-number effects.

1. Introduction

The objective of this paper is to investigate the ability of the large-eddy simulation (LES) technique to predict the principal characteristics of the shear-free turbulent boundary layer. This flow is of considerable interest, because one can study the inhibiting effects of the wall on an initially isotropic turbulent flow field independent of the effects of mean strain.

Previous work on this flow involves experiments performed by Uzkan & Reynolds (1967) in a water tunnel and, more recently, by Thomas & Hancock (1977) in a wind tunnel. Both experiments involve decaying grid turbulence passed over a wall moving at the same speed as the mean flow. Moreover, the problem has been dealt with theoretically by Hunt & Graham (1978).

In their experiments, conducted at a low Reynolds number (Re), Uzkan & Reynolds found that the turbulent fluctuations tangential to the surface (u_1) were *reduced* in amplitude by the presence of the wall. Their low-Reynolds-number analysis showed that the thickness of the inhomogeneity layer affected by the wall would grow as $(\nu t)^{\frac{1}{2}}$ (corresponding to growth proportional to $[\nu x_1/(U_e)_1]^{\frac{1}{2}}$ in the experiments); U_1 is the mean velocity in the tangential (streamwise) x_1 direction, ν is the kinematic viscosity, and subscript e refers to external flow conditions. In contrast, Thomas and Hancock's experiments, conducted at high Reynolds number, revealed tangential fluctuations near the surface of *greater* amplitude than in the free stream.

Hunt & Graham's theoretical work provides the explanation of these differences. They used a two-layer asymptotic analysis to predict the length scales, variances, and the one-dimensional power spectra of the fluctuating velocities. They assumed weak turbulence in the outer flow, $(u_e)_1 \ll (U_e)_1$ and $Re = (\overline{u_e^2})_1^{\frac{1}{2}} L_e/\nu \gg 1$, where u_1 is the fluctuating velocity in the x_1 direction and L is the integral length scale. With these assumptions, they employed boundary-layer approximations and modelled the

† Present address: Nielsen Engineering & Research, Inc., Mountain View, California 94043.

0022-1120/81/4611-2930 $02.00

flow in terms of an inner (viscous) layer scaling on $[\nu x_1/(U_e)_1]^{\frac{1}{2}}$ and an outer (source) layer scaling on L_e. The thickness of the (rotational) viscous layer was defined in terms of the normal component of the fluctuating vorticity, $(\omega_\nu)_2$. The vorticity of the source region was assumed to equal the vorticity of the external flow; hence $(\omega_s)_i = 0$ for all i. The solution for the linearized equations of the inner region gives $\delta_\nu = 4{\cdot}0[\nu x_1/(U_e)_1]^{\frac{1}{2}}$ for the thickness of the viscous layer. The outer-region solution was obtained by using a rapid distortion analysis.

Hunt & Graham compared their solutions with the data of Thomas & Hancock at $(Re)_M = (U_e)_1 M/\nu \sim 10^5$, where M is the grid spacing. Their predictions are in good overall agreement with experimental results, but fail to predict the Reynolds-number dependence of the u_1 amplification, and they overpredict the u_3 amplification in the source layer close to the wall. In addition, their theory is applicable only to large-Reynolds-number flows in which $\delta_\nu/L_e \ll 1$ and cannot predict the near-wall decay of u_1 in the low-Reynolds-number experiment ($Re_M \sim 10^3$) of Uzkan & Reynolds. In this experiment $\delta_\nu \sim \delta_s$, where δ_s is the thickness of the source layer, so that the large-Reynolds-number assumption of their theory is not valid.

In order to explain the streamwise dependence of the u_1 fluctuations observed in their experiment but not predicted by Hunt & Graham, Thomas & Hancock used a Reynolds-number-dependent dynamical model equation in which they incorporated Uzkan & Reynolds' results. Their predictions are in good agreement with their measurements, especially with respect to the increase in u_1 with streamwise distance and, hence, with increasing Reynolds number.

Because of the striking differences between the high- and low-Reynolds-number behaviour in this flow, it forms an excellent test base for turbulence modelling. Our objective here is to see if a new approach, large-eddy simulation (LES), is capable of predicting the observed effects over a wide Reynolds-number range. In § 2 we explain the LES procedure, in § 3 we present and discuss the results, and in § 4 we make some concluding remarks.

2. The calculation procedure

In large-eddy simulation of turbulent flows, each flow variable is decomposed into a large-scale component and a residual-field component. This can be obtained by filtering the flow variables (Leonard 1974) such that

$$u_i(\mathbf{x}, t) = \bar{u}_i(\mathbf{x}, t) + u_i'(\mathbf{x}, t) \tag{1}$$

and

$$\bar{u}_i(\mathbf{x}, t) = \int_D G(\mathbf{x}-\mathbf{x}')\mathbf{u}_i(\mathbf{x}', t)\,dx'. \tag{2}$$

In these expressions u_i' is the residual-field component, $\bar{u}_i$ is the large-scale (filtered) component, and $G(\mathbf{x}-\mathbf{x}')$ is the filter function. In previous simulations of homogeneous turbulence, we have used a Gaussian filter,

$$G(\mathbf{x}-\mathbf{x}') = \left[\left(\frac{\gamma}{\pi}\right)^{\frac{1}{2}}\frac{1}{\Delta}\right]^3 \exp\left[-\gamma(\mathbf{x}-\mathbf{x}')^2/\Delta^2\right], \tag{3}$$

where γ is a constant and Δ is the filter width. Kwak, Reynolds & Ferziger (1975) used $\gamma = 6$ and showed that by taking Δ as twice the computational mesh size, h, the best

results are obtained; calculations performed with the turbulent model constant that gives the proper energy decay, accurately predicted the filtered spectrum only when Δ was set equal to $2h$.

Application of filtering to the incompressible Navier–Stokes equations yields

$$\frac{\partial \overline{u}_i}{\partial t} + \overline{\overline{u}_j \left(\frac{\partial \overline{u}_i}{\partial x_j} - \frac{\partial \overline{u}_j}{\partial x_i} \right)} = -\frac{\partial P^*}{\partial x_i} - \frac{\partial}{\partial x_j} \tau_{ij} + \nu \frac{\partial^2 \overline{u}_i}{\partial x_k \partial x_k}, \tag{4}$$

where τ_{ij} represents the residual (subgrid scale – SGS) stresses and reads

$$\tau_{ij} = R_{ij} - \tfrac{1}{3} R_{kk} \delta_{ij}, \tag{5a}$$

$$R_{ij} = \overline{u_i' u_j'} + \overline{u_i' \overline{u}_j} + \overline{\overline{u}_i u_j'} \tag{5b}$$

and P^* is

$$P^* = \frac{\overline{p}}{\rho} + \tfrac{1}{3} R_{kk} + \tfrac{1}{2} \overline{(\overline{u}_k \overline{u}_k)}. \tag{5c}$$

In these equations $\overline{p}$ is the filtered pressure and ρ is the density.

It can be shown (Mansour *et al.* 1977) that the form of the convective terms in (4) will ensure conservation of momentum and energy in the absence of viscous terms for a broad range of finite-difference schemes including the scheme used in this work. This prevents the occurrence of nonlinear instability in the numerical solution procedure.

The closure will be obtained once the residual-stress field is defined in terms of the large-scale field. To this end we use the Smagorinsky (1963) model which has been successfully applied by Kwak *et al.* (1975), Mansour *et al.* (1977), and Ferziger, Mehta & Reynolds (1977) to the large-eddy simulation of homogeneous, isotropic turbulence and more recently to free shear flows by Mansour, Ferziger & Reynolds (1978) and the plane channel flow by Moin, Reynolds & Ferziger (1978*a*). Application of the LES to the calculation of homogeneous, isotropic turbulence (Kwak *et al.* 1975) with the use of the Smagorinsky model along with the proper model constant enabled the correct prediction of the rate of decay of filtered energy and the correct form of the energy spectrum. Use of the same model in the LES simulation of the plane channel flow (Moin *et al.* 1978*a*) resulted in successful predictions of the time-averaged mean-velocity profile as well as distributions of the resolvable Reynolds-stress components. The Smagorinsky model is

$$\tau_{ij} = -2\nu_T \overline{S}_{ij}, \tag{6a}$$

$$\nu_T = (C_s \Delta)^2 (2\overline{S}_{ij} \overline{S}_{ij})^{\frac{1}{2}}. \tag{6b}$$

It should be noted that this model is essentially an eddy-viscosity model where the characteristic length is expressed in terms of the grid length. In (6*a*) and (6*b*) $\overline{S}_{ij}$ denotes the strain-rate tensor of the large-scale field,

$$\overline{S}_{ij} = \frac{1}{2} \left(\frac{\partial \overline{u}_i}{\partial x_j} + \frac{\partial \overline{u}_j}{\partial x_i} \right). \tag{6c}$$

Also, C_s is a constant whose value can be estimated from spectral considerations (Lilly 1967) or evaluated by direct numerical experiment (Kwak *et al.* 1975; Clark, Ferziger & Reynolds 1977). In these numerical experiments, calculations were run with different values of the model constant and the value that predicted the rate of decay of the filtered energy most closely was selected. In view of these LES

calculations of the decay of isotropic, homogeneous turbulence, in this work we have used $C_s = 0{\cdot}2$.

Together with the Poisson equation for the pressure,

$$\nabla^2 P^* = \frac{\partial}{\partial x_i}\left[-\overline{\bar{u}_j\left(\frac{\partial \bar{u}_i}{\partial x_j} - \frac{\partial \bar{u}_j}{\partial x_i}\right)} + \frac{\partial}{\partial x_j}(2\nu_T \bar{S}_{ij})\right], \tag{7}$$

equations (4)–(7) can be numerically integrated once an initial velocity field and appropriate boundary conditions are prescribed.

In this work we employed a numerical integration code developed by Moin *et al.* (1978*a*) for the LES of plane channel flow. We calculated the flow field between two boundaries at $x_2 = 0$ and at $x_2 = D$, where D is the flow region. The boundary conditions will be described shortly.

The method of integration invokes flow homogeneity in the streamwise-x_1 and the lateral-x_3 directions by imposing periodic boundary conditions to expand the flow variables in terms of finite Fourier series, e.g. $\bar{u}_i$ can be written as

$$\bar{u}_1(x_1, x_2, x_3) = \sum_{n_1}\sum_{n_3} \hat{\bar{u}}_1(k_1, x_2, k_3)\exp[i(k_1 x_1 + k_3 x_3)],$$
$$n_l = -\tfrac{1}{2}N_j, \ldots, 0, 1, \ldots, \tfrac{1}{2}N_j - 1, \tag{8}$$

and the Fourier transform of $\bar{u}_1$ is given by

$$\hat{\bar{u}}_1(k_1, x_2, k_3) = \frac{1}{N_1 N_3}\sum_{m_1}\sum_{m_3} \bar{u}_1(x_1, x_2, x_3)\exp[-i(k_1 x_1 + k_3 x_3)], \quad m_l = 0, 1, \ldots, N_j - 1. \tag{9}$$

In expressions (8) and (9), $k_l = 2\pi n_l / N_j h_j$, h_j is the grid spacing in the x_j direction, whereas N_j is the number of mesh points in the x_j direction. The derivatives in x_1 and x_3 directions that appear in (4) are evaluated by the pseudospectral method (Fox & Orszag 1973) in which expansions (8) and (9) are used in conjunction with the fast-Fourier-transform algorithm of Singleton (1967). The derivatives in the inhomogeneous x_2 direction are evaluated by second-order central differences.

In this calculation the field variables can be filtered explicitly in the homogeneous directions (x_1 and x_3), and we modified (3) accordingly. Hence, for equal filter width, Δ, in the x_1 and x_3 directions,

$$G(\mathbf{x} - \mathbf{x}') = \left[\left(\frac{\gamma}{\pi}\right)^{\frac{1}{2}}\frac{1}{\Delta}\right]^2 \exp\left\{-\frac{\gamma}{\Delta^2}[(x_1 - x_1')^2 + (x_3 - x_3')^2]\right\}, \tag{10}$$

The finite differencing in the x_2 direction provides the filtering in this direction implicitly.

The second-order Adams–Bashforth method is used for explicit time advancement; $\bar{u}_i$ at time step $n+1$ is expressed as

$$\bar{u}_i^{n+1} = \bar{u}_i^n + \Delta t(\tfrac{3}{2}H_i^n - \tfrac{1}{2}H_i^{n-1}) \tag{11}$$

where

$$H_i = -\overline{\bar{u}_j\left(\frac{\partial \bar{u}_i}{\partial x_j} - \frac{\partial \bar{u}_j}{\partial x_i}\right)} - \frac{\partial P^*}{\partial x_i} - \frac{\partial}{\partial x_j}\tau_{ij} + \nu\frac{\partial^2 \bar{u}_i}{\partial x_k \partial x_k}. \tag{12}$$

The Poisson equation (7) solution selects a pressure that will ensure that $\bar{u}_i^{n+1}$ will be divergence-free. The Poisson equation is numerically integrated by a semi-direct method which employs Fourier transforms in the x_1 and x_3 directions and finite differences in the x_2 direction. This gives a pentadiagonal matrix in the x_2 direction owing to the five-point difference approximation. The calculation was carried out

for the time-evolving problem, which was then compared with the spatially evolving experiment by replacing t by $x_1/(U_e)_1$.

A random isotropic initial field was generated using the technique developed by Kwak *et al.*, outlined here. In wavenumber space, the definitions of the correlation tensor and its Fourier transform lead to

$$\hat{\bar{u}}_j(\mathbf{k}) = |\hat{\bar{u}}_j(\mathbf{k})\hat{\bar{u}}_j^*(\mathbf{k})|^{\frac{1}{2}}(aA_j + ibB_j) \tag{13}$$

and

$$\hat{\bar{u}}_j(\mathbf{k})\hat{\bar{u}}_j^*(\mathbf{k}) = \left(\frac{2\pi}{D}\right)^3 \frac{\bar{E}(\mathbf{k})}{2\pi k^2}, \tag{14}$$

where $\bar{E}(k)$ is the three-dimensional filtered spectrum, k is the shell-averaged wavenumber, $a = \cos\theta$, $b = \sin\theta$, and θ is a random angle, whereas D is the length of the computational box. A_j and B_j are unit vectors chosen randomly but are such that continuity is satisfied. Further, to make the velocity field real, $\hat{\bar{u}}_j(-\mathbf{k})$ was set equal to $\hat{\bar{u}}_j^*(\mathbf{k})$, where $*$ denotes complex conjugate. Then $\bar{u}_j(\mathbf{x})$ was obtained by inverse transforming $\hat{\bar{u}}_j(\mathbf{k})$. This procedure requires the prescription of an initial three-dimensional energy spectrum. In the present computations, this was obtained from the measured one-dimensional spectra of u_1 at a reference x_1-station taken as corresponding to time t_0. The three-dimensional spectrum, $E(k)$, was obtained from the measured one-dimensional spectrum, $F_{11}(k_1)$ from (Tennekes & Lumley 1972, p. 253)

$$E(k) = k_1^3 \frac{d}{dk_1}\left[\frac{1}{k_1}\frac{dF_{11}(k_1)}{dk_1}\right]. \tag{15}$$

It should be noted that this relationship holds for three-dimensional isotropy.

In all the calculations reported here we used a $16 \times 18 \times 16$ mesh to limit the computation time. We generated the initial field for a $16 \times 16 \times 16$ mesh system and placed this field inside our computational box. One extra point was then added at each x_2 boundary and values were imposed there to satisfy the required boundary conditions. After one time step, the flow field becomes divergence-free at all mesh points because of the solution process.

For the low Reynolds number of the Uzkan & Reynolds experiment, we imposed no-slip conditions at the lower wall ($x_2 = 0$) and no-stress conditions at the upper boundary ($x_2 = D$) to simulate flow conditions at a surface sufficiently far away from the solid wall:

$$\bar{u}_i = 0, \quad \text{at} \quad x_2 = 0; \tag{16a}$$

$$\bar{u}_2 = \frac{\partial \bar{u}_1}{\partial x_2} = \frac{\partial \bar{u}_3}{\partial x_2} = 0, \quad \text{at} \quad x_2 = D. \tag{16b}$$

In the high-Reynolds-number experiments of Thomas & Hancock, $\delta_\nu \ll \delta_s$, and hence all their measurements were taken outside the viscous layer. Since our computational mesh was not fine enough to resolve the viscous layer, we prescribed no-stress conditions at $x_2 = 0$ as well for the high-Reynolds-number simulation. It should be noted that in the source layer $(\omega_s)_i = 0$ and by continuity $u_2 = 0$ at the inner edge of the source layer, i.e. as $x_2/L \to 0$ (Hunt & Graham 1978). Hence, the no-stress conditions are the physically correct conditions to be imposed at the inner boundary for the high-Reynolds-number case. Periodic boundary conditions were used in the x_1 and x_3 directions.

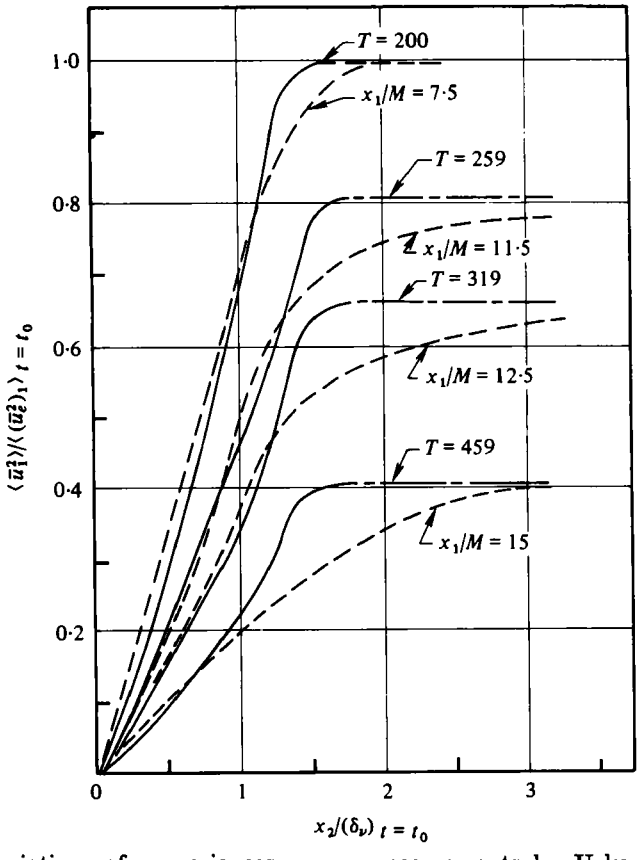

FIGURE 1. Variations of u_1 variances; – – –, measurements by Uzkan & Reynolds (1967); ——, present computations.

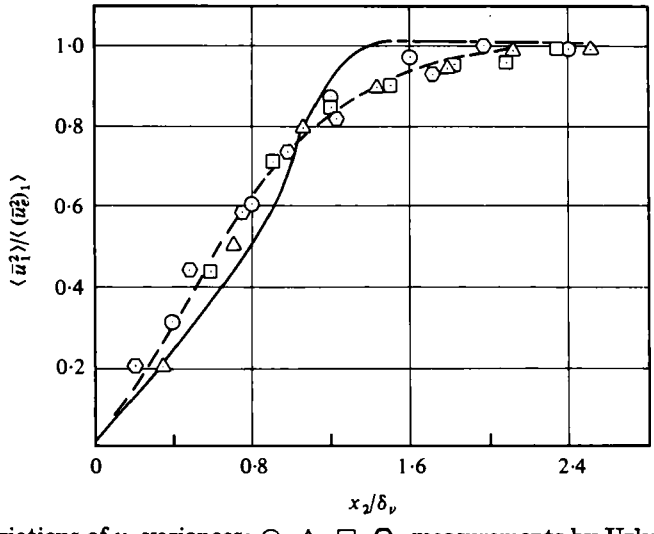

FIGURE 2. Variations of u_1 variances; ○, △, □, ⬡, measurements by Uzkan & Reynolds (1967) at $x_1/M = 7{\cdot}5$, $x_1/M = 11{\cdot}5$, $x_1/M = 12{\cdot}5$ and $x_1/M = 15$ respectively; – – –, average line through measurements; ——, present computations.

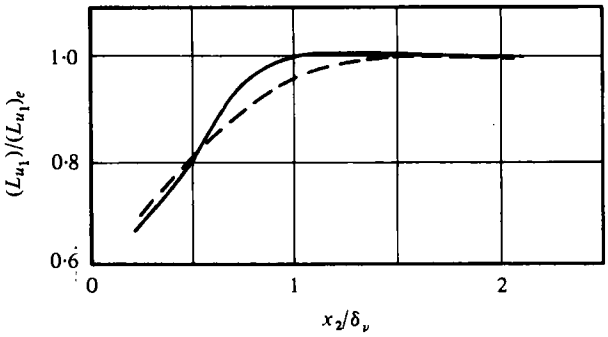

FIGURE 3. Variations of L_{u1}; – – –, measurements by Uzkan & Reynolds (1967); ——, present computations.

3. Results and discussion

All the computations were performed on a CDC-7600 at NASA-Ames Research Center. We used $C_s = 0{\cdot}2$, as in our earlier homogeneous-flow calculations. We define the characteristic Reynolds number in terms of the integral length scale, $(L_{u_1})_e$ and the r.m.s. value of $(u_e)_1$. This gives $Re \simeq 40$ for the Uzkan & Reynolds experiment and $Re \simeq 2000$ for the Thomas & Hancock experiment at $x_1/M = 22$. We also define the physical thickness of the viscous and source layers, δ_ν and δ_s, respectively, to be the x_2 co-ordinate at which the variances of $\overline{u}_1$ (in the case of δ_ν) and $\overline{u}_2$ (in the case of δ_s) reach 75 % of their free-stream values.

3.1. *Low-Reynolds-number case*

For the Uzkan & Reynolds experiment we chose the size of our computational box by assigning the grid spacing $h = 0{\cdot}15$ cm in all three directions. This resolves the energy spectrum for wavenumbers $2{\cdot}6 < k_1 < 21$ cm^{-1} and, considering the measured spectra for this flow, is adequate to capture most of the turbulence energy. The initial velocity field was generated from the measured one-dimensional energy spectrum of u_1 at the station $x_1 = 15$ inches (or $x_1/M = 7{\cdot}5$). For time advancement, we used $\Delta T = 0{\cdot}003$, where T is time non-dimensionalized by the reference length and velocity scales of the flow. This choice of the time step gives a Courant number which is well within the limits of stability requirements.

In order to obtain a smoothly varying field, the initial turbulent field had to be allowed to develop for about 200 time steps. It was then rescaled to the proper energy to match the experiment, and the calculation was continued for about 300 additional time steps. The corresponding times in the experiments were estimated using the Taylor hypothesis, and the experimental convection velocity was taken as $(U_e)_1$.

Results for the variances of the resolvable scale u_1-fluctuations are presented in figures 1 and 2, where we define the variance, e.g. $\langle \overline{u}_1^2 \rangle$, as a planar average in the x_1, x_3 plane. In figure 1 we use δ_ν and $\langle (\overline{u}_e^2)_1 \rangle$ at $t = t_0$ (or at $x_1/M = 7{\cdot}5$) as the scaling parameters. The computational curves display the same qualitative behaviour as the measured profiles, but the agreement between the two worsens with downstream distance because our computation does not produce the observed rate of growth of

the layer. We believe this failure is due to the close proximity of the upper boundary in the simulation.

As indicated by the dashed-dot lines (extensions of the computations), the rate of decay of free-stream turbulence energy is quite accurately predicted by the calculations.

In figure 2 we show the u_1 variances using the local values of δ_ν and $\langle(\overline{u}_e^2)_1\rangle$ as the scaling parameters. The computational curves follow the self-similar trend displayed by the measurements and confirm the error-function distributions of Uzkan & Reynolds.

Near the wall, the quantitative discrepancy between the shape of the computed curve in figure 2 and the measurements is likely to be due to excess extraction of energy by the SGS model; as yet we have not repeated the calculations with the modified wall-region SGS model of Moin *et al.* (1978*a*, *b*).

In figure 3 we plot the variation of the integral length scale, L_{u_1}, across the flow field. The integral length scale is defined as

$$L_{u_1} = \frac{U}{4\overline{u}_1^2} F_{11}(k_1)_{k\to 0}. \tag{17}$$

We compute $F_{11}(k_1)$ from

$$F_{11}(k_1) = \frac{1}{N_1}\sum_{n_1} \hat{\overline{u}}_1(k_1, x_2, x_3)\hat{\overline{u}}_1^*(k_1, x_2, x_3). \tag{18}$$

According to our mesh system, $n_1 = 1, \ldots, N_1$ and $N_1 = 16$. Hence one can calculate $L_{u_1}/(L_{u_1})_e$ from

$$\frac{L_{u_1}}{(L_{u_1})_e} = \frac{F_{11}(k_1)_{k_1\to 0}}{[F_{11}(k_1)_e]_{k\to 0}} \frac{\langle(\overline{u}_e^2)_1\rangle}{\langle\overline{u}_1^2\rangle}, \tag{19}$$

by extrapolating $F_{11}(k_1)$ to zero frequency.

The computed curve (figure 3) displays good qualitative agreement with the measured distribution. The computed length scale increases slightly and then decreases towards the wall. The experiment does not show the increase, but otherwise the agreement is quite satisfactory.

3.2. *High-Reynolds-number case*

In order to simulate the Thomas & Hancock experiment, we generated the initial field from the measured spectrum of u_1 at $x_1/M = 22$. The measurements at $x_1/M = 25$ are the target of our computations. We found it necessary to modify the initial conditions so as to produce a smooth field satisfying the boundary conditions at $x_2 = 0$. This was accomplished by multiplying the initial u_2 field by $\exp(-x_2^2)$. Again, after one time step the flow field becomes divergence-free.

In these computations we used $T = 0{\cdot}001$ for numerical stability and chose $h = 1{\cdot}5$ cm. This yields $0{\cdot}26 < k_1 < 2{\cdot}1$ cm^{-1} and captures most of the turbulence energy. The number of time steps necessary to cover the distance of 25 cm between the two experimental stations is about 350. In this high-Reynolds-number case, our computations displayed an irregular behaviour of the u_1, u_2 and u_3 variances over a considerable portion of the computational domain, even when the computations were carried to about 800 time steps. We attribute this to the persistence of the randomness of the initial field owing to insufficient statistical sampling. To increase the statistical

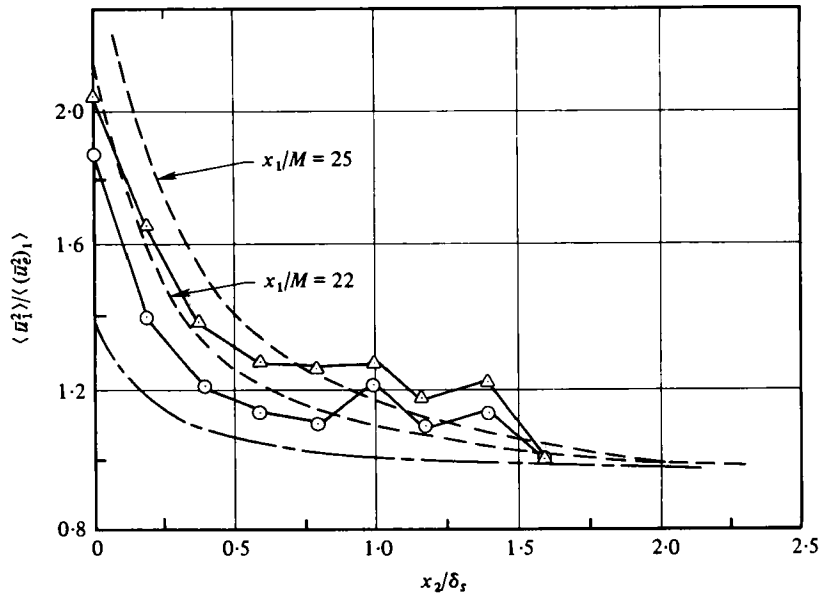

FIGURE 4. Variations of u_1 variances; – – –, measurements by Thomas & Hancock (1977); ○, present computations at $T = 10$; △, present computations at $T = 360$; ——–, theory of Hunt & Graham (1978).

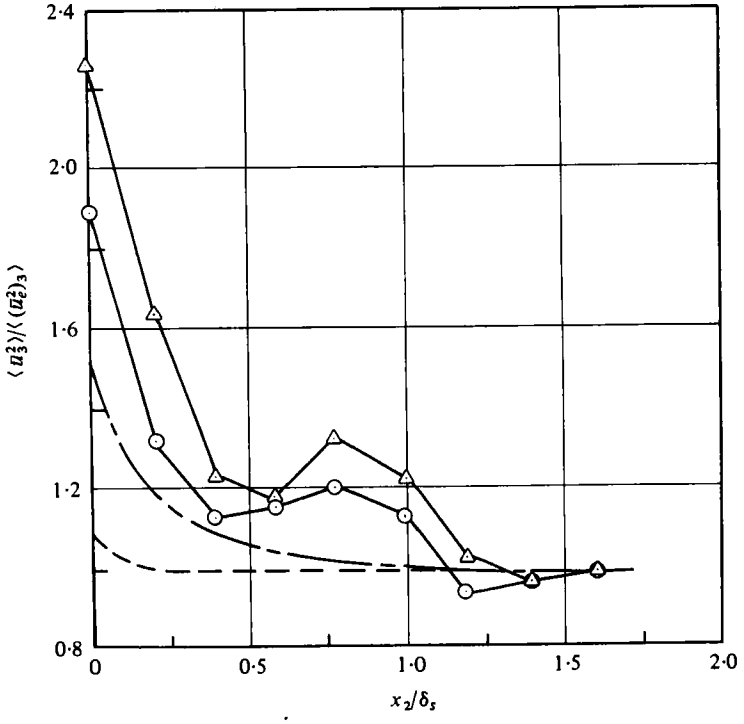

FIGURE 5. Variations of u_3 variances; symbols as in figure 4.

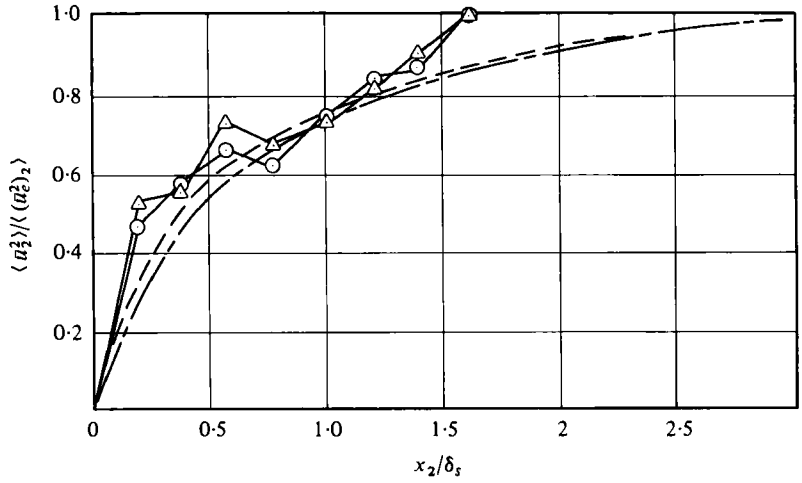

FIGURE 6. Variations of u_2 variances; symbols as in figure 4.

sampling, we created six different random fields as our initial conditions and ensemble-averaged the resulting variances. The averaged results are considerably smoother, and we conclude that the degree of smoothness of the distributions will increase with the number of samples.

In figures 4, 5 and 6 we compare the results of our computations with the Thomas & Hancock experiment at $x_1/M = 25$ and the predictions of Hunt & Graham. In these figures we use the local values of δ_s and $\langle (\bar{u}_e^2)_1 \rangle$ as the scaling parameters and take the edge of the flow to coincide with the half-thickness of the computational domain; all distributions are relatively flat at this point. It should be noted that, in the case of u_1 variances, the experiments of Thomas & Hancock show a marked deviation from self-similarity and that the amplification of u_1 fluctuations as well as the thickness of the source layer increases with downstream distance. Our computations also show some deviation from self-similarity, and the measurements are closely predicted over a considerable portion of the flow field. Near the wall, the computed values of u_1 variances are less than the experimental values, but much of the observed increases in amplitude is predicted.

Figure 5 shows a plot of the u_3 variances; note that the computed values are significantly higher than the measurements, especially close to the wall. Our calculations simulate grid-generated isotropic turbulence starting from isotropic initial conditions and assuming homogeneity in x_1 and x_3. Hence in the source region it should be expected that $\langle \bar{u}_1^2 \rangle = \langle \bar{u}_3^2 \rangle$, and our calculations closely predict this. The discrepancy between the measurements and our results are likely due to the existence of a preferred direction, x_1, in the measurements, which is not simulated in our calculations.

Finally, in figure 6 we present a plot of the u_2 variances (normal fluctuations). Except for the irregular behaviour around the centre of the flow field, which can be attributed to insufficient statistical sampling, the predictions compare favourably with experiment. Also, the computed results display a more abrupt increase than that indicated by the measurements.

4. Summary

We now summarize the main conclusions of this work.

(1) Large-eddy simulation of the shear-free turbulent boundary layer has predicted the primary Reynolds-number effects on the behaviour of the tangential turbulence variances near the wall – damping at low Reynolds number and amplification at high Reynolds number.

(2) Comparisons with the low-Reynolds-number experiments suggest that the SGS model should be modified to provide less energy extraction near the wall.

This work was supported in part by the NASA/Ames Research Center. The senior author was on leave from the Boğaziçi University on an AID fellowship during the period of this work. The helpful assistance and advice of Professor Parviz Moin and Professor Joel Ferziger are greatly appreciated.

REFERENCES

CLARK, R. A., FERZIGER, J. H. & REYNOLDS, W. C. 1977 *Dept. Mech. Engng, Stanford Univ. Rep.* TF-9.

FERZIGER, J. H., MEHTA, U. B. & REYNOLDS, W. C. 1977 *Proc. Symp. on Turbulent Shear Flows, Penn. State Univ.*

FOX, D. G. & ORZSAG, S. A. 1973 *J. Comp. Phys.* **11**, 612.

HUNT, J. C. R. & GRAHAM, J. M. R. 1978 *J. Fluid Mech.* **84**, 209.

KWAK, D., REYNOLDS, W. C. & FERZIGER, J. H. 1975 *Dept. Mech. Engng Stanford Univ. Rep.* TF-5.

LEONARD, A. 1974 *Adv. Geophys.* A **18**, 237.

LILLY, D. K. 1967 *Proc. IBM Scientific Computing Symp. on Environmental Sciences*, p. 195.

MANSOUR, N. N., MOIN, P., REYNOLDS, W. C. & FERZIGER, J. H. 1977 *Proc. Symp. on Turbulent Shear Flows, Penn. State Univ.*

MANSOUR, N. N., FERZIGER, J. H. & REYNOLDS, W. C. 1978 *Dept. Mech. Engng Stanford Univ. Rep.* TF-11.

MOIN, P., REYNOLDS, W. C. & FERZIGER, J. H. 1978*a* *Dept. Mech. Engng Stanford Univ. Rep.* TF-12.

MOIN, P., MANSOUR, N. N., REYNOLDS, W. C. & FERZIGER, J. H. 1978*b* *Proc. 6th Int. Conf. on Numerical Methods in Fluid Dynamics, Tbilisi, U.S.S.R.* (to be published).

SINGLETON, R. C. 1967 *Communications of the ACM* **10**, 647.

SMAGORINSKY, J. 1963 *Monthly Weather Rev.* **93**, 99.

TENNEKES, H. & LUMLEY, J. L. 1972 *A First Course in Turbulence.* Massachusetts Institute of Technology Press.

THOMAS, N. H. & HANCOCK, P. E. 1977 *J. Fluid Mech.* **82**, 481.

UZKAN, T. & REYNOLDS, W. C. 1967 *J. Fluid Mech.* **28**, 803.